ORIGINAL PAPER

Tribological Behavior of Carbon Nanotube-Reinforced AZ91D Composites Processed by Cyclic Extrusion and Compression

Li Zhang[1] · Qudong Wang[1] · Guoping Liu[1] · Wei Guo[1] · Bing Ye[1] · Wenzhen Li[2] · Haiyan Jiang[1] · Wenjiang Ding[1]

Abstract

Reciprocating wear tests were conducted to assess the wear resistance of CNT-reinforced AZ91D composites prepared by cyclic extrusion and compression (CEC). Effects of CEC, CNTs, and wear parameters on the tribological behavior of the composites were discussed. Results show that the matrix grain of the 0.5 wt% CNTs/AZ91D composites is largely refined from ~112 μm to 126.6 nm after eight passes of CEC. Accordingly, the hardness of the composites is increased by more than 82.0%. The wear rate of the CNTs/AZ91D composites decreases with the implement of CEC and the addition of CNTs. The lubrication effect of CNTs diminishes after CEC. Besides the reinforcing effect, the incorporated CNTs help to liberate the friction heat of the CNTs/AZ91D composites and reduce the welding of the wear debris due to their extraordinary thermal conductivity.

Keywords Magnesium composites · Carbon nanotubes · Cyclic extrusion compression · Wear mechanism

1 Introduction

Years of efforts have enabled Mg alloys to be competitive candidates in areas where weight reduction is critical, such as aerospace and automotive industries. However, the low thermal stability and poor wear resistance limit their wider applications in situations where the sliding motion occurs [1–4]. To combat these issues, various methods, including alloying with rare-earth elements (RE) [5–8] and incorporating of different kinds of reinforcements [9–12], have been made. By adding 3 wt% of RE into AZ91, the wear rate of AZ91+3RE alloy was reported to be 50% lower than that of the base alloy at room temperature [6]. A similar result was obtained by Lim et al. [9] that compared with pure-Mg, the wear resistance of the 1.11 vol% nano-Al_2O_3-reinforced Mg composites was increased up to 1.8 times. The basic principle of these methods is to increase the wear resistance of

Mg alloys by increasing their load-bearing capacities. One of the undesirable facts is that during the sliding process, the detached or crushed hard RE-containing intermetallics or ceramic particles may cause surface damage by acting as abrasive particles, which accelerates the failure of the matrix [13]. However, this is not the case for carbon nanotubes (CNTs), since either partially or fully crushed CNTs may form a carbon film which covers the worn surface and acts as solid lubricants [14–16]. Meanwhile, CNTs possess an extraordinary thermal conductivity, implying that the friction heat generated could be effectively dissipated and the thermal softening of the Mg matrix would be reduced [17–19]. Therefore, CNTs are a preferential choice in the designing of Mg composites with high wear resistance.

Severe plastic deformation (SPD) has long been taken as an effective technique in the dispersing of nano-reinforcements due to its large accumulated strain and abundant materials flow [20, 21]. To date, successful attempts to fabricate nano-reinforced composites by SPD include high-pressure torsion (HPT) [22, 23], accumulated roll bonding (ARB) [24, 25], and friction stir processing (FSP) [26, 27]. Besides the greatly refined microstructure and enhanced mechanical properties, wear properties of the SPD-processed composites were reported to be superior to their unprocessed counterparts. Darmiani et al. [24] reported that after six passes of ARB, the incorporated nano-SiC particles were uniformly

✉ Qudong Wang
wangqudong@sjtu.edu.cn

1 National Engineering Research Center of Light Alloy Net Forming and State Key Laboratory of Metal Matrix Composites, School of Materials Science and Engineering, Shanghai Jiao Tong University, Shanghai 200240, China

2 School of Materials Science and Engineering, Tsinghua University, Beijing 10084, China

distributed within the Al matrix and the wear resistance of the nano-SiC/Al composites increased with the progress ARB. FSP was used by Lu et al. [26] to process nano-Al_2O_3 and CNT-reinforced AZ31 composites. Results show that the microhardness of the FSP stirred area was higher than that of the surrounded areas, and the wear resistance of the hybrid composites was increased greatly after the implement of FSP.

Although SPD is a feasible technique both in preparing the CNT-reinforced composites and in enhancing the wear resistance of the composites, limited works [1, 26, 27] have been done on Mg and no work has been done with the implement of cyclic extrusion and compression (CEC), which is suggested as a superior technique in the processing of the hard-to-deform materials [28, 29]. Thus, CEC was used to prepare the CNT-reinforced AZ91D composites in this work. Effects of CEC, CNTs and wear parameters on the tribological behavior of the composites were then discussed.

2 Materials and Methods

The matrix alloy used was Mg–8.66Al–0.56Zn–0.16Mn (designated as AZ91D) and the reinforcement incorporated was multi-walled CNTs with a diameter of 20–40 nm and length of 1–5 µm. Magnesium matrix composites containing 0.5 and 2.0 wt% of CNTs were fabricated by ultrasonic cavitation-assisted casting, followed by a solution treatment at 413 °C for 24 h. Prior to the implement of CEC, the billets were machined into cylindrical rods with dimensions of $\Phi 30\,mm \times 42\,mm$ by an electric discharge machine (EDM).

The schematic illustration and detailed procedures of CEC can be found in our recent published works [28, 29]. CEC was conducted at 300 °C for eight passes in this study. The monolithic AZ91D alloy was also prepared in the same way for comparison.

Microstructure of the CNTs/AZ91D composites was examined by optical microscopy (OM, Olympus XJL-30) and scanning electron microscopy (FE-SEM, Sirion 200) equipped with an energy dispersive spectrometer (EDS, INCA X-MAX80). A standard metallographic technique, including mechanical grinding with 320, 1200, 3000, and 5000 grit SiC paper and final polishing with a magnesia suspension, was used in the sample preparation. The etchant used was a mixture of 1 ml nitric acid, 1 ml acetic acid, 1 g oxalic acid, and 150 ml water.

Hardness tests were conducted using a Vickers indenter under a load of 49 N and a dwell time of 15 s. Eight different indentations along the longitudinal section were then taken and averaged for each sample.

Dry sliding wear tests were carried out on a reciprocating friction and wear test machine, the installation of which was given in Fig. 1. Wear samples were machined along the longitudinal direction with dimensions of 35 mm×6 mm×4 mm and the counter stationary ball used was GGr15 steel with a diameter of 10 mm. Each sample was ultrasonically cleaned with alcohol for 20 min both before and after the test. An electronic balance with an accuracy of 0.1 mg was used to measure the wear loss. Wear tests were conducted at room temperature with a sliding speed of 0.15 m/s under a normal load of 8 N for a sliding distance of 2000 m. Effects of the load were revealed under loads of 4
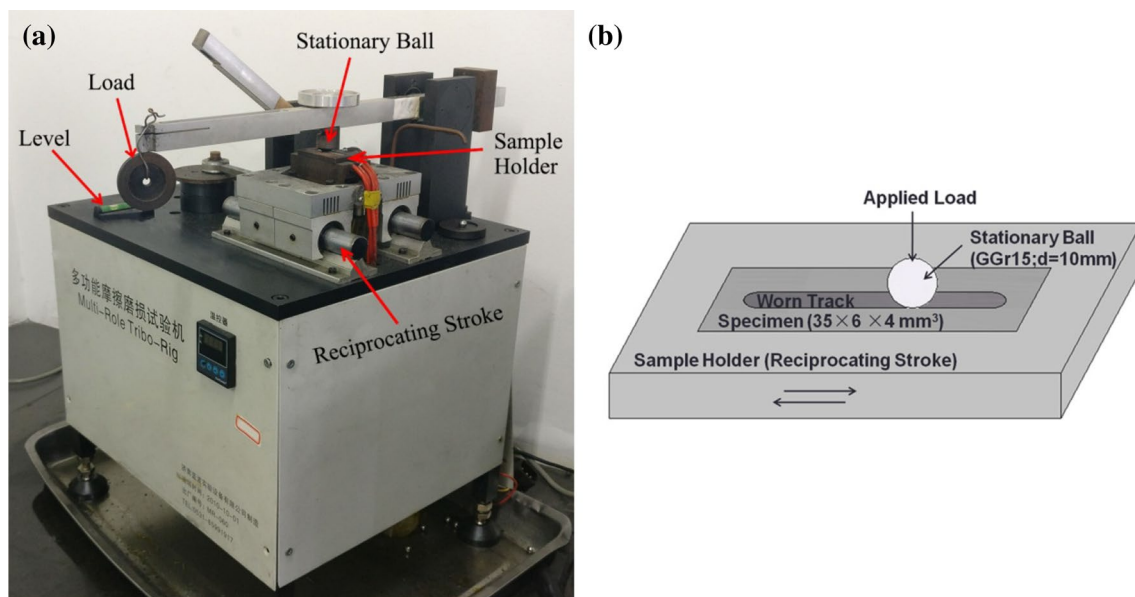

Fig. 1 **a** Experiment setup of the reciprocating wear test and **b** installation of the wear specimens

and 12 N at a sliding speed of 0.15 m/s, and the effects of the sliding speeds were elucidated by additional tests at 0.10 and 0.20 m/s under a load of 8 N. Coefficient of friction (COF) was automatically recorded with the sliding distance. Worn surfaces and the cross-sectional structures were examined by SEM and EDS.

Thermal conductivity (λ) was calculated through the following equation [30]:

$$\lambda = \alpha \times \rho \times C_p, \tag{1}$$

where α is the thermal diffusivity (mm^2/s), ρ is the density (g/cm^3), and C_p is the specific heat capacity (W/(m K)). The thermal diffusivity (α) was measured using a laser flash apparatus (LFA 447, NETZSCH) and the specific heat capacity (C_p) was obtained using a differential scanning calorimetry (DSC 8000). Densities of the composites (ρ) were calculated according to the mixture rule [14] by considering the density of AZ91D alloy being 1.82 g/mm^3 and that of CNTs 1.73 g/mm^3.

3 Results and Discussion

3.1 Microstructures

Microstructure of the initial solution-treated 0.5CNTs/AZ91D composites is given in Fig. 2a. It is apparent that the matrix grain of the fabricated composites is homogeneous with a size of ~ 112 μm and the majority of second phases dissolve after the solution treatment, leaving a small amount of $Mg_{17}Al_{12}$ and Mn-rich (mainly Al_8Mn_5) particles [29]. The incorporated CNTs are highly agglomerated as shown in Fig. 2b, which is mainly attributed to their large surface-to-volume ratio and poor wettability with the Mg matrix. After eight passes of CEC, the matrix grain of the 0.5CNTs/AZ91D composites is greatly refined down to ~ 126.6 nm (Fig. 2c) and $Mg_{17}Al_{12}$ second phases are uniformly precipitated along grain boundaries. The initial CNT-clusters are effectively dispersed into an extended area after the implement of CEC, but the length-to-diameter ratio is greatly shortened as shown in Fig. 2d. Degrading of CNTs after the implement of SPD is also reported by other researchers [17–19, 29].

Effects of CNTs on the microstructural characteristics of both the solution-treated and CEC-processed alloy/
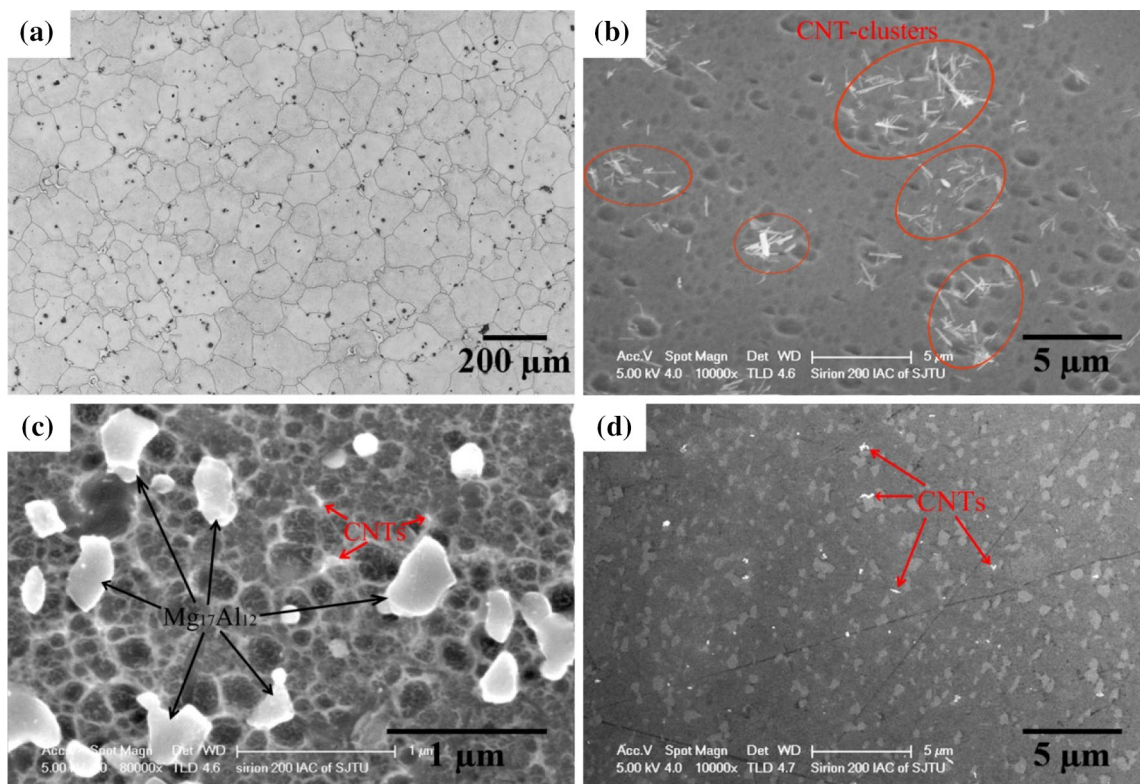

Fig. 2 Microstructures of the **a, b** solution-treated and **c, d** eight-pass CEC-processed 0.5CNTs/AZ91D composites, with **b, d** giving the distribution of CNTs within the Mg matrix

composites are compared in Table 1. It is apparent that the incorporated CNTs lead to a reduced matrix grain not only for the initial samples but also for those after the implement of CEC. As for $Mg_{17}Al_{12}$ precipitates, the similar particle size and area fraction suggest that CNTs exert a negligible effect on the precipitation of $Mg_{17}Al_{12}$.

3.2 Hardness

Hardness of the solution-treated and the CEC-processed alloy/composites are tabulated in Table 1. Compared with the solution-treated base alloy, even 2.0 wt% of CNTs lead to a trivial increase of ~6.5% in the hardness of the solution-treated CNTs/AZ91D composites. This inefficient reinforcing effect is believed to be related with the highly agglomerated CNTs. Eight-pass of CEC induces huge increments of ~53.1, ~82.0, and ~64.2% in the hardness of the AZ91D base alloy, 0.5CNTs/AZ91D and 2.0CNTs/AZ91D composites, respectively. These remarkable increments should be attributed to the greatly refined matrix grain and the extensively precipitated $Mg_{17}Al_{12}$ after the implement of CEC. Besides, composites reinforced by CNTs exhibit a superior hardness than that of the monolithic alloy. Though the 2.0CNTs/AZ91D composites posses a finer matrix grain and a larger amount of CNTs, the corresponding hardness is lower than that of the 0.5CNTs/AZ91D composites. As reported in Ref. [29], the severely degraded CNTs may act as or introduce various kinds of crystal defects within the matrix, which undermines the strength of the composites.

3.3 Wear

3.3.1 Coefficient of Friction (COF)

The variations of COF with the increasing of sliding distance for the solution-treated and CEC-processed alloy/composites under wear conditions of 0.15 m/s and 8 N are shown in Fig. 3a, b, respectively. It is apparent that after a short running-in stage, COF increases steady with the sliding distance. This is reasonable since the contact surface of the friction pairs is gradually damaged with the progress of wear and thus the interaction would be intensified accordingly

[31]. For the solution-treated samples, COF curves almost coincide with the initial sliding distance of ~300 m. From this point on, the COF curves separate from each other, with the monolithic alloy giving the highest COF (0.263) and the 2.0CNTs/AZ91D composites exhibiting the lowest COF (0.203), indicating that CNTs could be effectively acted as the solid lubricant and thus contribute to the reduction of COF. Besides, the COF curve of the 2.0CNTs/AZ91D composites fluctuates greatly compared with the other two, which is consistent with the observed inhomogeneous distribution of CNTs within the Mg matrix. In contrast, COF curves of the CEC-processed AZ91D alloy, 0.5CNTs/AZ91D, and 2.0CNTs/AZ91D composites are found to be similar throughout the wear test, with the mean COF values being 0.193, 0.191, and 0.192, respectively. It seems that the lubrication effect provided by CNTs diminishes after the implement of CEC. The degraded CNTs after CEC should be responsible for this observation.

Regardless of the amount of the incorporated CNTs, the CEC-processed samples exhibit a lower COF than their solution-treated counterparts. For example, COF of the unprocessed 0.5CNTs/AZ91D composites covers a relative wide range of 0.190–0.263 with a mean value of 0.235, while that of the CEC-processed composites falls into the range of 0.186–0.226 with a mean value of 0.191. This suggests that the implement of CEC could effectively reduce COF of the friction pairs, which is mainly attributed to the huge increased hardness resulting from the ultrafine-grained matrix and the extensively precipitated $Mg_{17}Al_{12}$.

For the CEC-processed 0.5CNTs/AZ91D composites, variations of COF depending on the applied load and the sliding speed are shown in Fig. 3c, d, respectively. At a sliding speed of 0.15 m/s, the COF curve obtained under the applied load of 4 N is obviously higher than those acquired under loads of 8 and 12 N. The mean COF of the post-processed 0.5CNTs/AZ91D composites decreases from 0.207 to 0.181 with the increasing of the applied loads up to 12 N. At an applied load of 8 N, the COF decreases continuously from 0.208 to 0.165 with the increasing of the sliding speed from 0.10 to 0.20 m/s. These reductions in COF with the increasing of the applied load and the sliding speed were commonly reported in other research works [14, 31], and the softening

Table 1 Microstructural characteristics and hardness of the alloy/composites both before and after the implement of CEC

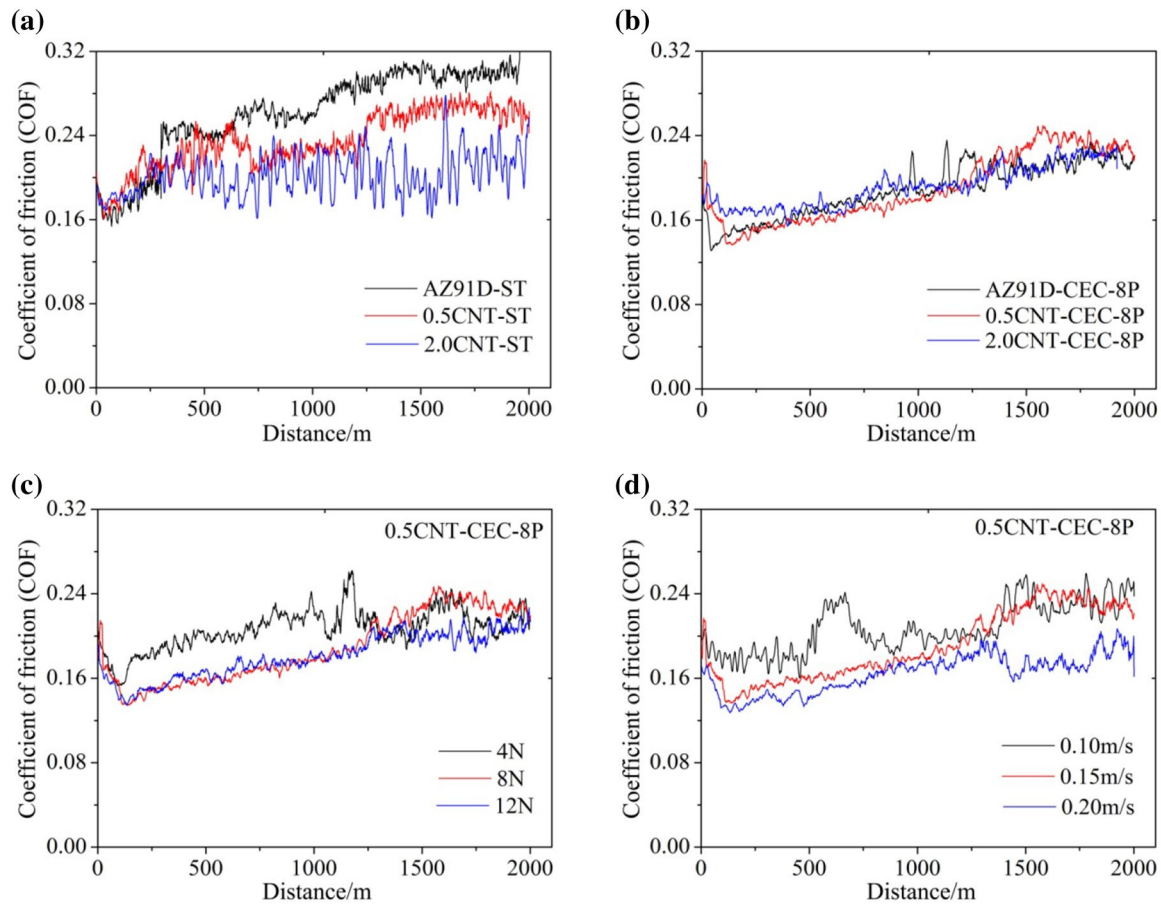| | Status | Matrix grain size | $Mg_{17}Al_{12}$ second phase | | Hardness/Hv |
			Size/µm	Area fraction/%	
AZ91D	ST	300 µm	–	–	57.12
	CEC-8P	140.9 nm	0.23	14.5	87.47
0.5CNTs/AZ91D	ST	112 µm	–	–	56.79
	CEC-8P	126.6 nm	0.24	14.3	103.36
2.0CNTs/AZ91D	ST	75 µm	–	–	60.86
	CEC-8P	106.5 nm	0.22	14.7	99.92

Fig. 3 Variations of coefficient of friction (COF) with the increasing of sliding distance for **a** the solution-treated alloy/composites under wear conditions of 0.15 m/s and 8 N, **b** the CEC-processed alloy/composites under wear conditions of 0.15 m/s and 8 N, **c** CEC-pro-cessed 0.5CNTs/AZ91D composites at the sliding speed of 0.15 m/s and **d** CEC-processed 0.5CNTs/AZ91D composites under the applied load of 8 N

induced by the friction hear under higher applied loads or at higher sliding speeds was concluded to be responsible for these variations.

3.3.2 Wear Loss

Effects of CNT additions on wear losses of the solution-treated and the CEC-processed alloy/composites under various wear conditions are shown in Fig. 4. A general view is that the wear loss decreases continuously with the increasing of CNT contents. Taking those tested with a sliding speed of 0.15 m/s and an applied load of 8 N (Fig. 4a) as examples, incorporations of 0.5 and 2.0 wt% of CNTs reduce the wear loss of the initial solution-treated base alloy by 5.09 and 13.20%, respectively. For those after the implement of CEC, a similar trend is observed and 2.0 wt% of CNTs induces an increment of ~16.99% in the wear resistance of the post-processed base alloy. Thus, the incorporated CNTs could enhance the wear resistance of the base alloy. Note that CNTs lead to a reduced COF for the solution-treated

composites, while a similar COF for the CEC-processed ones. Thus, the dominant role played by CNTs may be different, which will be discussed in Sect. 3.3.3.

As for the effect of CEC, as shown in Fig. 4a, compared with the solution-treated samples, their CEC-processed counterparts exhibit lower wear losses. Specifically, after the implement of CEC, wear losses of the AZ91D alloy, 0.5CNTs/AZ91D, and 2.0CNTs/AZ91D composites are decreased by 3.24, 8.29, and 7.47%, respectively. These decrements in mass loss can be explained by considering the greatly increased hardness and the decreased COF as stated above.

Mass losses of the CEC-processed alloy/composites at a sliding speed of 0.15 m/s under various loads are shown in Fig. 4b. As expected, increasing in the applied load intensifies the interaction between the friction pairs and thus leads to an increase in the wear loss. Effects of the sliding speed on the mass loss of the post-processed samples under a normal load of 8 N are given in Fig. 4c. It is apparent that the wear loss decreases with the increasing of the sliding speed
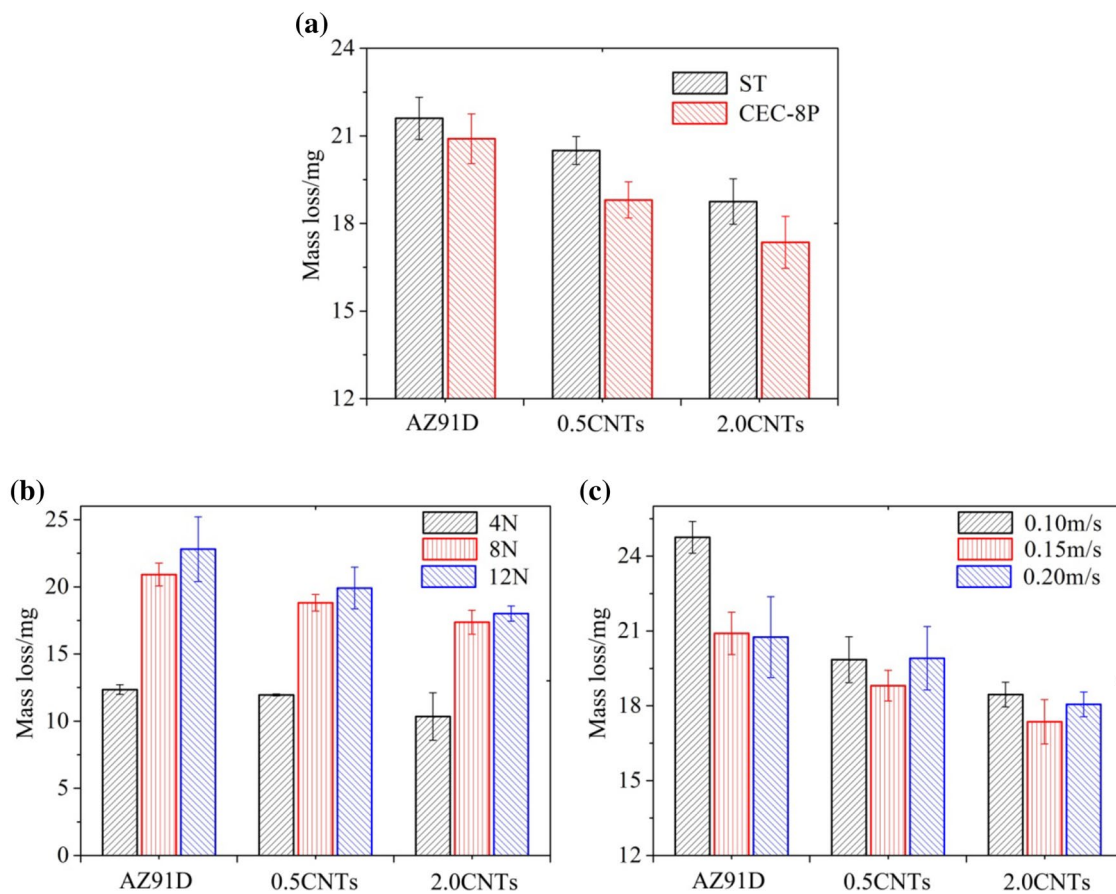
(a)

(b)

(c)

Fig. 4 Wear mass loss for **a** the solution-treated and CEC-processed alloy/composites under wear conditions of 0.15 m/s and 8 N, **b** CEC-processed alloy/composites at the sliding speed of 0.15 m/s and **c** CEC-processed alloy/composites with the applied load of 8 N

from 0.10 to 0.15 m/s, while an opposite trend is observed with the sliding speed further increasing to 0.20 m/s, implying that the wear mechanism operated may alter with the increasing of the sliding speed [32].

3.3.3 Worn Surface

Worn surfaces of the solution-treated and the CEC-processed 0.5CNTs/AZ91D composites under wear conditions of 0.15 m/s and 8 N are shown in Fig. 5a, b, respectively. Large craters and cracks are observed in the worn surface of the solution-treated 0.5CNTs/AZ91D composites, indicating adhesion and delamination are the major wear mechanisms [25, 33, 34]. However, grooves and scratches, typical characters of the abrasive wear [34], are observed in the composites after eight passes of CEC. EDS results of typical points on the worn surfaces of the 0.5CNTs/AZ91D composites are given in Fig. 5c, d. Though being situated in a newly formed crater, P1 still exhibits 5.09 wt% of oxygen, suggesting that the affinity of magnesium to oxygen is extremely high and oxidation occurs

during the wear test [35, 36]. This is also the case for the post-processed sample, since 14.65 wt% (P2) of oxygen is detected in its worn surface. Besides, wear debris of the solution-treated sample is generally separated in the form of large flakes or plates, while that of the CEC-processed sample is gradually abraded in the form of fine particles. The corresponding EDS analysis (Fig. 5e, f) reveals that the main constituents of the wear debris are Mg and MgO. And it is believed that the detached MgO may penetrate into the worn surface and act as abrasive particles that would induce extra scratches [13].

Worn surfaces and the corresponding subsurface layers of the post-processed alloy/composites tested with a sliding speed of 0.15 m/s under an applied load of 8 N are shown in Figs. 6, 7, respectively. Surface pits can be readily found on the worn surface of the AZ91D alloy and wear debris tend to be accumulated within those surface pits. With the increasing of CNT contents, worn surfaces of the composites seem to be featureless with shallow grooves and fine scratches. The most distinct feature between the AZ91D alloy and the CNTs/AZ91D composites exists in their
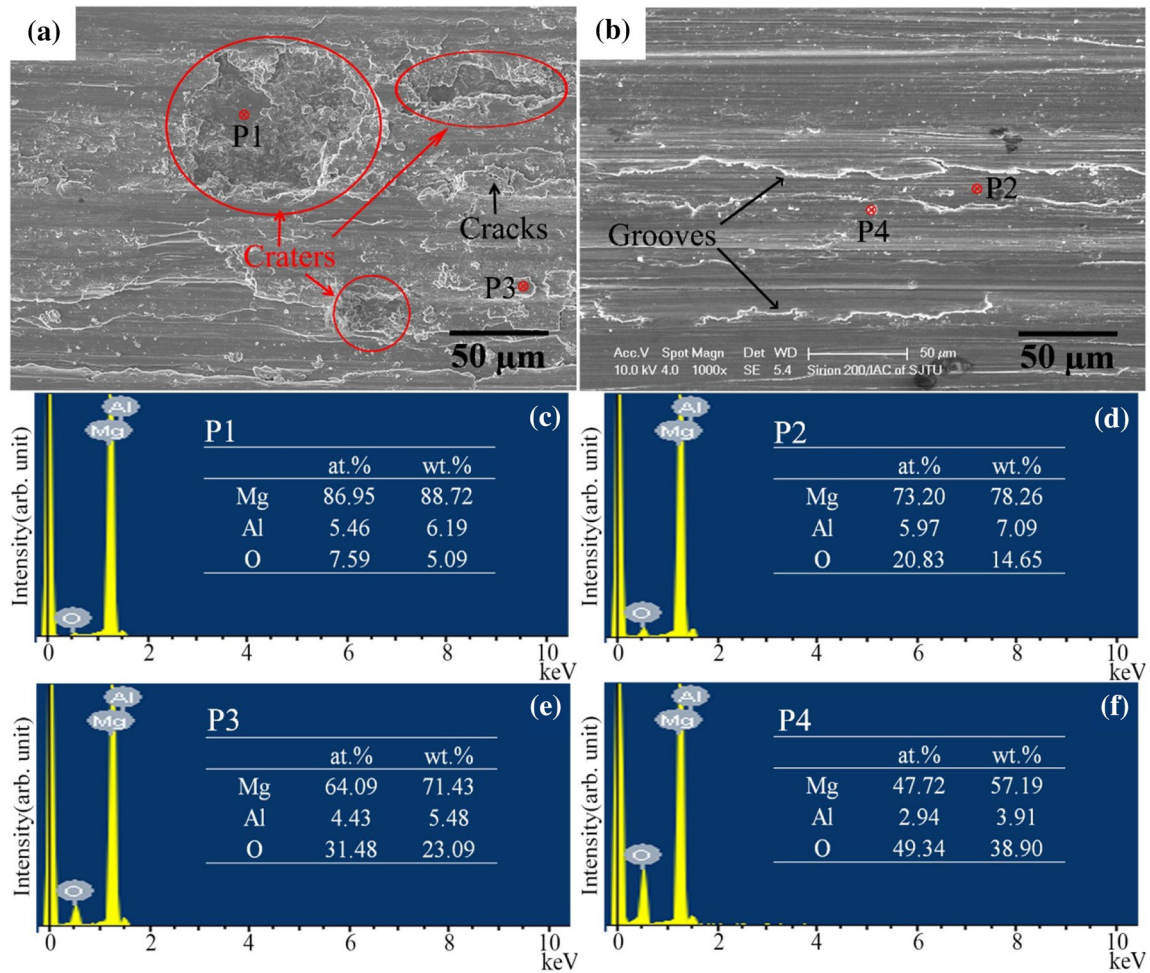
Fig. 5 Worn surfaces of the **a** solution-treated and **b** CEC-processed 0.5CNTs/AZ91D composites under wear conditions of 0.15 m/s and 8 N, with **c, d, e, f** giving the EDS results of P1, P2, P3, and P4, respectively
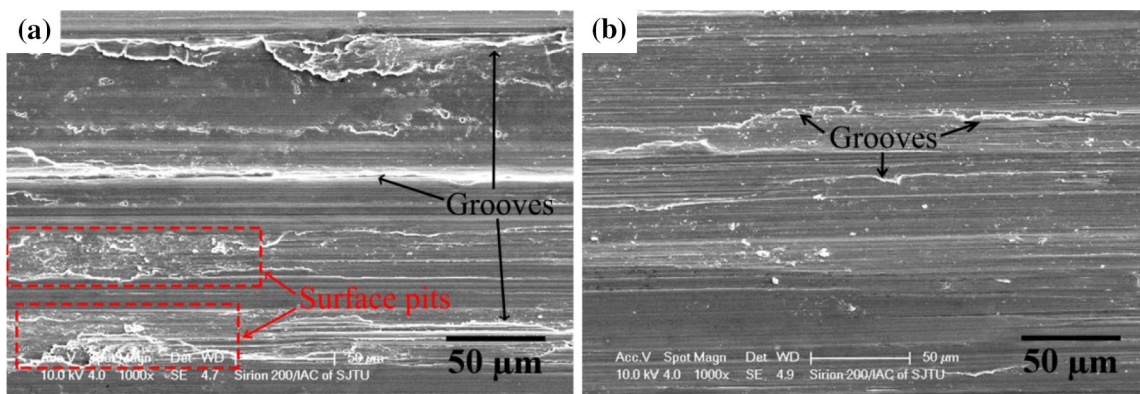

Fig. 6 Worn surfaces of the eight-pass CEC-processed **a** monolithic AZ91D alloy and **b** 2.0CNTs/AZ91D composites under wear conditions of 0.15 m/s and 8 N

subsurface structures. Unlike the continuous tribo-oxide layer (as indicated in Fig. 5c) on the topmost surface of the composites, the subsurface structure of the monolithic alloy is discontinuous and made up by some detached particles. Subsequent EDS analysis (Fig. 7b, c) reveals that the chemical constituent of this layer is similar to that of the wear
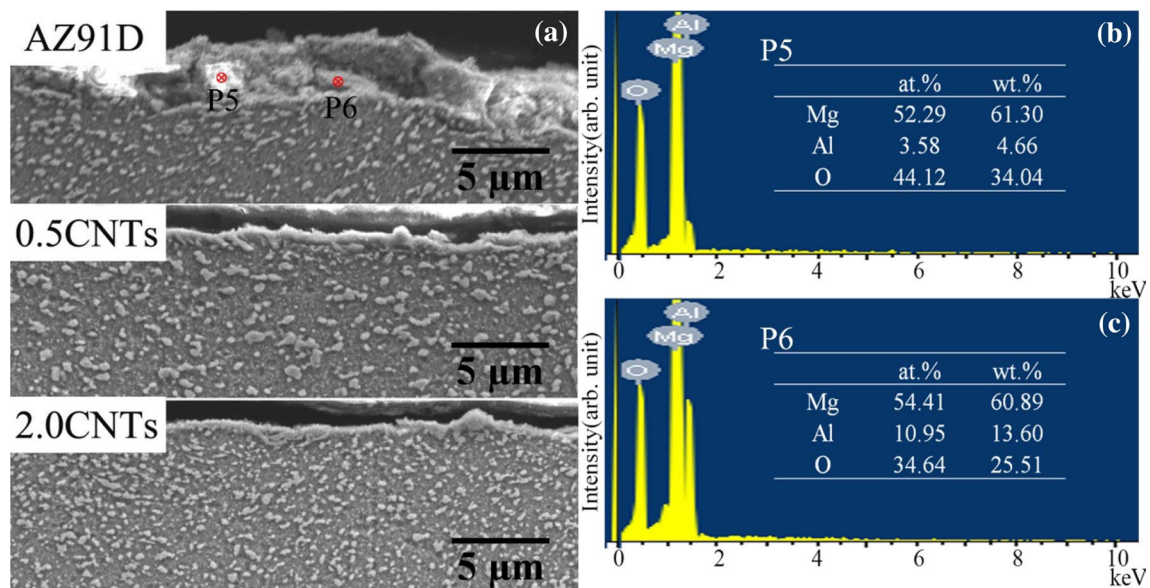
Fig. 7 **a** Subsurface layers of the eight-pass CEC-processed monolithic alloy and composites tested with a sliding speed of 0.15 m/s under an applied load of 8 N, with **b, c** giving the EDS results of P5 and P6, respectively
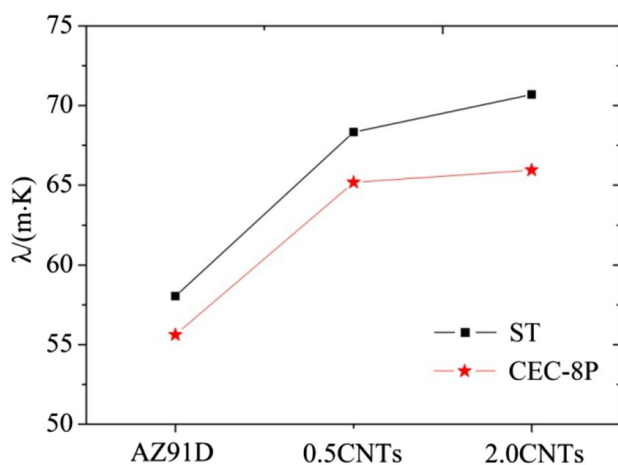

Fig. 8 Thermal conductivities of the solution-treated and eight-pass CEC-processed alloy and composites

debris. Therefore, this discontinuous tribo-layer is deduced to be tightly compacted or welded wear debris.

Generally, the localized welding of wear debris is caused by their plastic deformation [26]. As discussed in Sect. 3.2, the monolithic AZ91D alloy shows a relatively lower hardness compared with that of the CNT-reinforced composites, which makes it favorable for the occurrence of plastic deformation. Besides, the mechanical properties of AZ91 alloy are rapidly degraded with the increasing of temperature, since $Mg_{17}Al_{12}$ softens and coarsens easily at elevated temperature [7, 37]. Friction heat generates inevitably during the reciprocating wear test, thus the temperature rise needs to be considered. Figure 8 gives thermal conductivities of

the monolithic AZ91D alloy and CNTs/AZ91D composites both before and after the implement of CEC. Though CNTs are ruptured after CEC, the thermal conductivities of the composites are still higher than that of the monolithic alloy, indicating that the friction heat generated could be effectively liberated in the composites with the help of CNTs. Therefore, during the reciprocating wear test, the contact temperature of the AZ91D alloy is higher than that of the composites, which leads to the softening of the monolithic alloy and facilitates the welding of wear debris [14].

Worn surface of the CEC-processed 0.5CNTs/AZ91D composites tested under various loads are given in Fig. 5b (8 N) and Fig. 9 (4 and 12 N). Under lower normal loads (< 8 N), the worn surfaces are featured by grooves and scratches, suggesting the abrasive wear as the dominant wear mechanism. However, plenty of cracks, which are nearly perpendicular to the sliding direction, appear on the worn surface when the normal load increases to 12 N. Generally, the appearance of cracks is associated with the occurrence of delamination. Meanwhile, as shown in Fig. 10, the typical characters of delamination [38], including the generation of a tribo-layer, nucleation and propagation of fatigue cracks in the subsurface, and final detachment of large plates, are observed in the subsurface layer obtained under the applied load of 12 N, which further verifies that delamination is the major wear mechanism at this applied load level. Therefore, the dominant wear mechanism alters from abrasion to delamination with the applied load increased from 8 to 12 N.

Effects of the sliding speeds on the worn surfaces and the corresponding subsurface layers of the post-processed 0.5CNTs/AZ91D composites are shown in Figs. 11, 12,
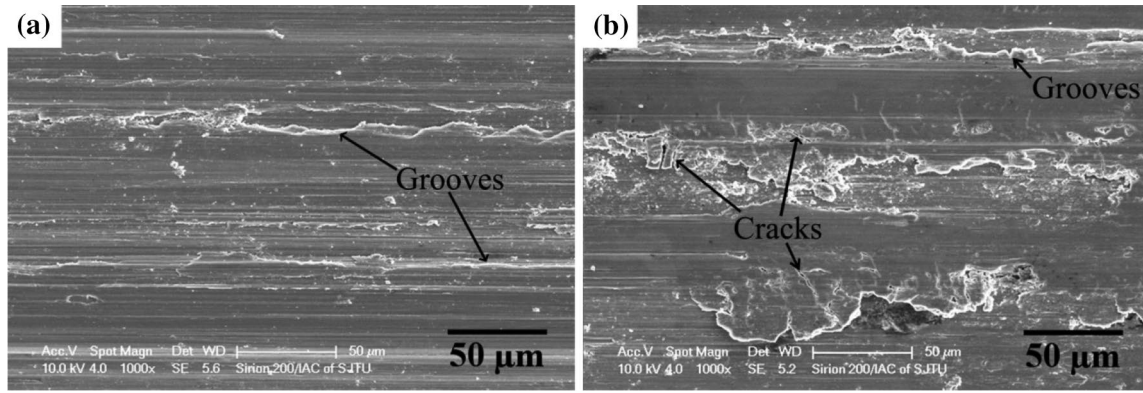
Fig. 9 Worn surfaces of the eight-pass CEC-processed 0.5CNTs/AZ91D composites tested with the sliding speed of 0.15 m/s under normal loads of **a** 4 N and **b** 12 N
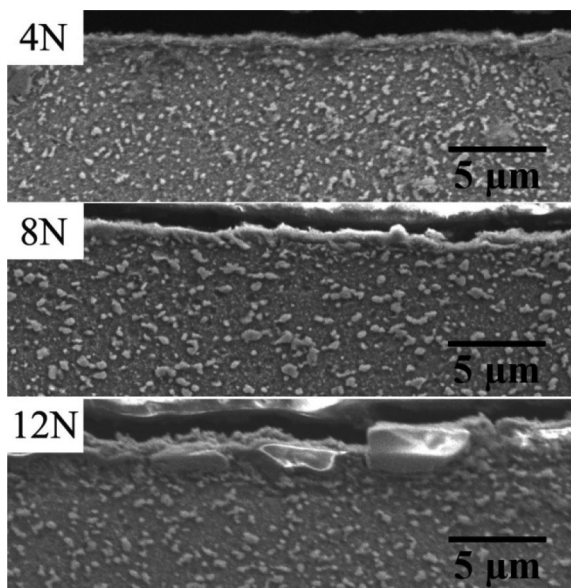

Fig. 10 Subsurface layers of the eight-pass CEC-processed 0.5CNTs/AZ91D composites tested with the sliding speed of 0.15 m/s under various loads

respectively. With the increasing of sliding speeds, the width between grooves decreases, while the thickness of the tribo-layer increases. When the sliding speed reaches 0.20 m/s, cracks and delaminated plates are observed. Thus, it can be deduced that the dominant wear mechanism alters from abrasion to delamination with the increasing of sliding speeds, which is consistent with our previous judgment that is based on the variation of wear loss with the sliding speed. This alternation in wear mechanism is believed to be related with the temperature rise within the contact area, since for a given sliding distance (2000 m in our case), increasing in the sliding speed results in less time for the friction heat to be dissipated, which raises the local temperature and degrades the mechanical properties of the composites [14, 37].

4 Conclusions

Reciprocating wear tests were carried out to study the wear resistance of CNT-reinforced AZ91D composites prepared by CEC. Effects of CEC, CNT additions, and wear
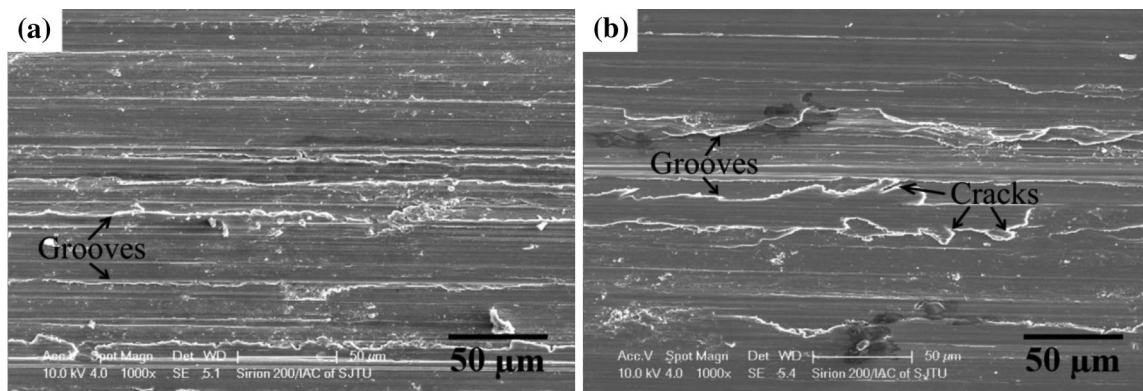

Fig. 11 Worn surfaces of the eight-pass CEC-processed 0.5CNTs/AZ91D composites tested at sliding speeds of **a** 0.10 and **b** 0.20 m/s under the applied load of 8 N
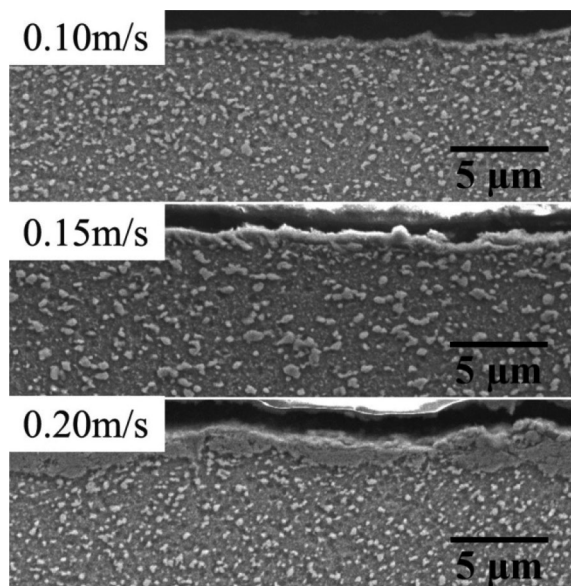
Fig. 12 Subsurface layers of the eight-pass CEC-processed 0.5CNTs/AZ91D composites tested at various sliding speeds under the applied load of 8 N

parameters on the wear behavior of the post-processed composites were then discussed. The following conclusions are drawn:

1. Eight passes of CEC refines the matrix grain of 0.5CNTs/AZ91D composites from 112 μm to 126.6 nm. $Mg_{17}Al_{12}$ second phases are dynamically precipitated along grain boundaries and the incorporated CNTs are dispersed into an extended area after the implement of CEC. All contribute to the huge increased hardness.
2. Compared with the original solution-treated samples, their CEC-processed counterparts exhibit lower wear losses. Wear loss decreases continuously with the increasing of CNT contents and 2.0 wt% of CNTs induces an increment of ~ 16.99% in the wear resistance of the post-processed alloy. Adhesion and delamination are the major wear mechanisms for the initial solution-treated samples, while abrasive wear is the dominant wear mechanisms for the CNTs/AZ91D composites. Oxidation occurs commonly during the wear test.
3. The lubrication effect of CNTs diminishes with the progress of CEC. But the extraordinary thermal conductivity of CNTs helps to liberate the generated friction heat, retain a reasonable strength for the CNTs/AZ91D composites, and reduce the welding tendency of the wear debris.
4. Increasing either in the applied load or in the sliding speed leads to an alternation of the dominant wear mechanism from abrasion to delamination. The critical

load and the critical sliding speed are 8 N and 0.15 m/s in this research work.

References

1. Arora, H.S., Singh, H., Dhindaw, B.K.: Wear behaviour of a Mg alloy subjected to friction stir processing. Wear **303**, 65–77 (2013)
2. An, J., Sun, W., Niu, X.D.: Dry sliding wear behavior and a proposed criterion for mild to severe wear transition of Mg–3Al–0.4Si–0.1Zn alloy. Tribol. Lett. **65**, 98 (2017)
3. An, J., Zhang, Y.X., Lv, X.X.: Tribological characteristics of Mg–3Al–0.4Si–0.1Zn alloy at elevated temperatures of 50–200 °C. Tribol. Lett. **66**, 14 (2017)
4. Babu, J., Anjaiah, M., Mathew, A.: Experimental studies on Friction stir processing of AZ31 Magnesium alloy. Mater. Today **5**, 4515–4522 (2018)
5. Nouri, M., Sun, X., Li, D.Y.: Beneficial effects of yttrium on the performance of Mg–3% Al alloy during wear, corrosion and corrosive wear. Tribol. Int. **67**, 154–163 (2013)
6. Zafari, A., Ghasemi, H.M., Mahmudi, R.: An investigation on the tribological behavior of AZ91 and AZ91+ 3 wt% RE magnesium alloys at elevated temperatures. Mater. Des. **54**, 544–552 (2014)
7. An, J., Li, R.G., Lu, Y., Chen, C.M., Xu, Y., Chen, X., et al.: Dry sliding wear behavior of magnesium alloys. Wear **265**, 97–104 (2008)
8. Keerti, S., Gokhale, A., Jain, J., Huang, E.-W.: Influence of Zn addition on micro-scale wear of Mg–xZn (x = 1–6 wt%) alloys. Tribol. Lett. **65**, 140 (2017)
9. Lim, C.Y.H., Leo, D.K., Ang, J.J.S., Gupta, M.: Wear of magnesium composites reinforced with nano-sized alumina particulates. Wear **259**, 620–625 (2005)
10. Nguyen, Q.B., Sim, Y.H.M., Gupta, M., Lim, C.Y.H.: Tribology characteristics of magnesium alloy AZ31B and its composites. Tribol. Int. **82**, 464–471 (2015)
11. Seenuvasaperumal, P., Elayaperumal, A., Jayavel, R.: Influence of calcium hexaboride reinforced magnesium composite for the mechanical and tribological behviour. Tribol. Int. **111**, 18–25 (2017)
12. García-Rodríguez, S., Torres, B., Maroto, A., López, A.J., Otero, E., Rams, J.: Dry sliding wear behavior of globular AZ91 magnesium alloy and AZ91/SiCp composites. Wear **390–391**, 1–10 (2017)
13. Moazami-Goudarzi, M., Akhlaghi, F.: Wear behavior of Al 5252 alloy reinforced with micrometric and nanometric SiC particles. Tribol. Int. **102**, 28–37 (2016)
14. Bastwros, M.M.H., Esawi, A.M.K., Wifi, A.: Friction and wear behavior of Al–CNT composites. Wear **307**, 164–173 (2013)
15. Choi, H.J., Kwon, G.B., Lee, G.Y., Bae, D.H.: Reinforcement with carbon nanotubes in aluminum matrix composites. Scr. Mater. **59**, 360–363 (2008)
16. Reinert, L., Varenberg, M., Mücklich, F., Suárez, S.: Dry friction and wear of self-lubricating carbon-nanotube-containing surfaces. Wear **406–407**, 33–42 (2018)
17. Tjong, S.C.: Recent progress in the development and properties of novel metal matrix nanocomposites reinforced with carbon nanotubes and graphene nanosheets. Mater. Sci. Eng. R Rep. **74**, 281–350 (2013)

18. Bakshi, S.R., Lahiri, D., Agarwal, A.: Carbon nanotube reinforced metal matrix composites—A review. Int. Mater. Rev. **55**, 41–64 (2010)

19. Dorri Moghadam, A., Omrani, E., Menezes, P.L., Rohatgi, P.K.: Mechanical and tribological properties of self-lubricating metal matrix nanocomposites reinforced by carbon nanotubes (CNTs) and graphene—A review. Compos. B **77**, 402–420 (2015)

20. Viswanathan, V., Laha, T., Balani, K., Agarwal, A., Seal, S.: Challenges and advances in nanocomposite processing techniques. Mater. Sci. Eng. R Rep. **54**, 121–285 (2006)

21. Li, X., Xu, J.: 6.5 Metal matrix nanocomposites. Comprehensive composite materials II, pp. 97–137. Elsevier, Amsterdam (2018)

22. Edalati, K., Ashida, M., Horita, Z., Matsui, T., Kato, H.: Wear resistance and tribological features of pure aluminum and Al–Al$_2$O$_3$ composites consolidated by high-pressure torsion. Wear **310**, 83–89 (2014)

23. Aal, M.I.A.E., Kim, H.S.: Wear properties of high pressure torsion processed ultrafine grained Al–7% Si alloy. Mater. Des. **53**, 373–382 (2014)

24. Darmiani, E., Danaee, I., Golozar, M.A., Toroghinejad, M.R., Ashrafi, A., Ahmadi, A.: Reciprocating wear resistance of Al–SiC nano-composite fabricated by accumulative roll bonding process. Mater. Des. **50**, 497–502 (2013)

25. Jamaati, R., Naseri, M., Toroghinejad, M.R.: Wear behavior of nanostructured Al/Al$_2$O$_3$ composite fabricated via accumulative roll bonding (ARB) process. Mater. Des. **59**, 540–549 (2014)

26. Lu, D., Jiang, Y., Zhou, R.: Wear performance of nano-Al$_2$O$_3$ particles and CNTs reinforced magnesium matrix composites by friction stir processing. Wear **305**, 286–290 (2013)

27. Lee, W.-B., Lee, C.-Y., Kim, M.-K., Yoon, J.-I., Kim, Y.-J., Yoen, Y.-M., et al.: Microstructures and wear property of friction stir welded AZ91 Mg/SiC particle reinforced composite. Compos. Sci. Technol. **66**, 1513–1520 (2006)

28. Zhang, L., Wang, Q., Liao, W., Guo, W., Ye, B., Li, W., et al.: Effects of cyclic extrusion and compression on the microstructure and mechanical properties of AZ91D magnesium composites reinforced by SiC nanoparticles. Mater. Charact. **126**, 17–27 (2017)

29. Zhang, L., Wang, Q., Liao, W., Guo, W., Li, W., Jiang, H., et al.: Microstructure and mechanical properties of the carbon nanotubes reinforced AZ91D magnesium matrix composites processed by cyclic extrusion and compression. Mater. Sci. Eng. A **689**, 427–434 (2017)

30. Pan, H., Pan, F., Yang, R., Peng, J., Zhao, C., She, J., et al.: Thermal and electrical conductivity of binary magnesium alloys. J. Mater. Sci. **49**, 3107–3124 (2014)

31. Choi, H.J., Lee, S.M., Bae, D.H.: Wear characteristic of aluminum-based composites containing multi-walled carbon nanotubes. Wear **270**, 12–18 (2010)

32. Aung, N.N., Zhou, W., Lim, L.E.N.: Wear behaviour of AZ91D alloy at low sliding speeds. Wear **265**, 780–786 (2008)

33. Mazaheri, Y., Karimzadeh, F., Enayati, M.H.: Tribological behavior of A356/Al$_2$O$_3$ surface nanocomposite prepared by friction stir processing. Metall. Mater. Trans. A **45**, 2250–2259 (2014)

34. Wilson, S., Alpas, A.T.: Wear mechanism maps for metal matrix composites. Wear **212**, 41–49 (1997)

35. Kim, I.Y., Lee, J.H., Lee, G.S., Baik, S.H., Kim, Y.J., Lee, Y.Z.: Friction and wear characteristics of the carbon nanotube–aluminum composites with different manufacturing conditions. Wear **267**, 593–598 (2009)

36. Czerwinski, F.: The oxidation behaviour of an AZ91D magnesium alloy at high temperatures. Acta Mater. **50**, 2639–2654 (2002)

37. Zafari, A., Ghasemi, H.M., Mahmudi, R.: Tribological behavior of AZ91D magnesium alloy at elevated temperatures. Wear **292–293**, 33–40 (2012)

38. Suh, N.P.: An overview of the delamination theory of wear. Wear **44**, 1–16 (1977)